To be submitted to
Nuovo Cimento

ISTITUTO NAZIONALE DI FISICA NUCLEARE
Laboratori Nazionali di Frascati

LNF-77/1(P)
3 Gennaio 1977

S. Bartalucci, S. Bertolucci, C. Bradaschia, M. Fiori, D. Fong, T. Mc Corriston, P. Giromini, S. Guiducci, C. Rippich, M. Rohde, A. Sermoneta and L. Trasatti: A SEARCH FOR NEW VECTOR MESONS IN THE MASS RANGE BETWEEN 0.9 AND 2.2 GeV.

Servizio Documentazione
dei Laboratori Nazionali di Frascati
Cas. Postale 13 - Frascati (Roma)

INFN - Laboratori Nazionali di Frascati
Servizio Documentazione

LNF-77/1(P)
3 Gennaio 1977

A SEARCH FOR NEW VECTOR MESONS IN THE MASS RANGE BETWEEN 0.9 AND 2.2 GeV.

S. Bartalucci, S. Bertolucci, C. Bradaschia, M. Fiori, D. Fong, T. Mc Corriston, P. Giromini, S. Guiducci, C. Rippich, M. Rohde, A. Sermoneta and L. Trasatti

Deutsches Elektronen Synchrotron DESY, Hamburg (Germany), and
Laboratori Nazionali di Frascati dell'INFN, Frascati (Italy).

SUMMARY: We have measured the yield of e^+,e^- pairs in the reaction $\gamma p \rightarrow p e^+ e^-$ in the invariant mass region $0.9 \lesssim M \lesssim 2.2$ GeV/c^2. The result, based on 2×10^4 events, shows with a statistical significance of 7 standard deviations a new resonance-like single structure with width $5 \lesssim \Gamma \lesssim 30$ MeV at $M \sim 1100$ MeV. For $1.2 \lesssim M \lesssim 1.8$ GeV the data exhibit an additional wide structure, which can be accounted for by two broad resonances at about 1400 and 1700 MeV. The existence of the $\varrho'(1250)$ and $\varrho''(1600)$ is neither proven nor excluded by the data.

1. - THEORETICAL BACKGROUND. -

We have carried out an experiment on the inclusive yield of e^+e^- pairs with the ?.2 GeV bremsstrahlung beam of the DESY electron synchrotron. The reaction

$$\gamma p \rightarrow p e^+ e^-$$

was studied by detecting the e^+ and e^- in the final state with a double arm magnetic spectrometer. The differential production rate for this process is given by

$$\frac{dN}{dp_+ dp_- d\Omega_+ d\Omega_-} = N_p N_{eq} \int dQ'^2 f(K) \left| A_T \right|^2 \qquad (1)$$

where + and - refer to the positron and electron respectively, N_p is the number of protons per cm^2 in the target, N_{eq} is the number of equivalent quanta collected, f(K) is the bremsstrahlung spectrum and Q' is the target recoil four-momentum.

The amplitude A_T is expressed by:

$$A_T = A_{BH} + A_C + \text{QED terms corresponding to diagrams in which the } e^+e^- \text{ pairs are connected to more than two } \gamma\text{-rays.} \qquad (2)$$

A_{BH}, the Bethe-Heitler amplitude, describes QED to the first order, according to the following diagrams:

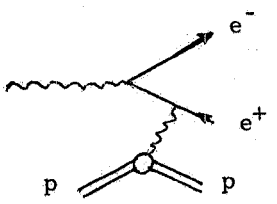

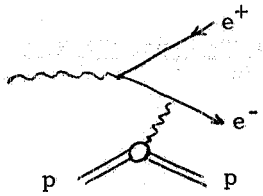

Following refs. (1) and (2) we write:

$$\left|A_{BH}\right|^2 = \frac{\alpha^3}{16\pi^2}\,\frac{E_+E_-}{(KQ)(KQ')}\,\frac{1}{q^4}\,\delta(Q'^2 - M_p^2)\,M_{\mu\nu}\left\{W_1^{el}\left(g^{\mu\nu} - \frac{q^\mu q^\nu}{q^2}\right) + W_2^{el}R^\mu R^\nu\right\}. \qquad (3)$$

Here K_μ is the incident photon four-momentum, M_p is the proton mass and q_μ is the momentum transfer of the pair. Q_μ and Q'_μ are the proton initial and final four momenta. $g^{\mu\nu}$ is the metric: 1, -1, -1, -1.

$$M_{\mu\nu} = \frac{-2}{\beta_+\beta_-}\,(\beta_+^2 + \beta_-^2 + 2M^2q^2)\,g_{\mu\nu} - \frac{8q^2}{\beta_+\beta_-}\,(p_{+\mu}p_{+\nu} + p_{-\mu}p_{-\nu}) +$$

$$+ 4m_e^2\left\{q^2\left(\frac{1}{\beta_+} + \frac{1}{\beta_-}\right)^2 g_{\mu\nu} + \left(\frac{2p_{-\mu}}{\beta_+} - \frac{2p_{+\mu}}{\beta_-}\right)\left(\frac{2p_{-\nu}}{\beta_+} - \frac{2p_{+\nu}}{\beta_-}\right)\right\},$$

where $\beta_\pm = 2Kp_\pm$ and $M^2 = (p_+ + p_-)^2$ and $R^\mu = \frac{Q^\mu + Q'^\mu}{2M_p}$.

Finally,

$$W_1^{el} = q^2\left|G_M\right|^2$$

$$W_2^{el} = 4M_p^2\left(\left|G_E\right|^2 - \tau\left|G_M\right|^2\right)/(1-\tau), \qquad \text{where} \quad \tau = q^2/4M_p^2.$$

The magnetic and electric form factors are related to each other by $G_M = 2.79\,G_E$. The measured value of the hydrogen elastic form factor from ref. (3) has been used to calculate the B H contribution.

Corrections due to inelastic Bethe-Heitler processes have been calculated by replacing in (3) $\delta(Q'^2 - M_p^2)$ with $1/2\pi$ and W_1^{el} and W_2^{el} with

$$W_1^{inel} = -\frac{x\,M_p}{\pi a}\,\sigma_\perp$$

$$W_2^{inel} = \frac{x\,M_p}{\pi a}\,(\sigma_\perp + \sigma_\parallel)/\left(1 - \frac{\nu^2}{q^2}\right).$$

Here $x = \frac{Q'^2 - M_p^2}{2M_p}$ and $\nu = x - \frac{q^2}{2M_p}$. $\sigma_\perp$ and $\sigma_\parallel$, which are functions of q^2 and Q'^2, are the transverse and longitudinal virtual photoproduction cross sections. Values of $\sigma_\perp$ and $\sigma_\parallel$ have been taken from refs. (2) and (4). Inelastic corrections have been found to be of the order of 10%.

Radiative corrections to the elastic Bethe-Heitler production have been calculated according to ref. (5) and found to be of the order of - 10%.

A_C in equation (2) is the Compton scattering amplitude, which is represented by the diagram

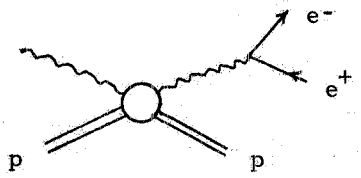

One has:

$$\left|A_C\right|^2 = \frac{\alpha^2}{4\pi^3}\frac{(KQ)}{(KQ')}E_+E_-(E_+E_- - P_{+z}P_{-z} + m_e^2)\left|\Lambda_C\right|^2 \delta(Q'^2 - M_P^2) \quad . \tag{4}$$

where z is the direction of the incoming photon.

In the framework of the vector dominance model, where the hadronic electromagnetic current is a linear combination of vector meson fields, Λ_C can be parametrized, assuming helicity conservation, as

$$\Lambda_C = i\Sigma_V \left(\frac{m_V^2}{M^2}\frac{e^{i\varphi_V}}{m_V^2 - M^2 - im_V\Gamma_V}\sqrt{\frac{d\sigma_V}{dt}\Big/\frac{\gamma_V^2}{4\pi}}\right) , \tag{5}$$

$$\frac{d\sigma_V}{dt} = \frac{d\sigma}{dt}(\gamma p \rightarrow Vp)\Big|_{t=0} e^{b_V t} \quad .$$

Here, m_V is the mass of the vector meson; $t = -q^2$, b_V is the slope of the cross-section for vector meson photoproduction on proton; $\varphi_V + \pi/2$ is the relative phase between the vector meson photoproduction amplitude and the B H amplitude; $\gamma_V^2/4\pi$ is the vector meson-photon coupling constant.

The interference term between the Bethe-Heitler and Compton amplitudes is given by:

$$2\,\mathrm{Re}\left\{A_{BH}A_C\right\} = \frac{(\alpha/\pi)^{5/2}}{4}\frac{E_+E_-}{q^2(KQ')}\delta(Q'^2 - M_p^2)\frac{MG_E}{\sqrt{1-\tau}}\Lambda\,\mathrm{Re}(\Lambda_C) \tag{6}$$

with

$$\Lambda = \frac{1}{2}\sum_\varepsilon\left(\frac{1}{\beta_+}\lambda(+,-) - \frac{1}{\beta_-}\lambda(-,+)\right) ,$$

and

$$-\frac{1}{2}\lambda(+,-) = \varepsilon\varepsilon'(M^2K + \beta_+E_- - \beta_-E_+) - \frac{(K\varepsilon')}{K}\left[\beta_-(p_+\varepsilon) - \beta_+(p_-\varepsilon)\right] -$$

$$- 4(K + E_- - E_+)(p_+\varepsilon)(p_-\varepsilon') .$$

Here ε and ε' are respectively the polarization four-vectors of the incoming photon and of the outgoing vector meson. Contributions due to the interference of A_{BH} with higher order QED terms have been estimated according to[6] to be about 0.1% of the elastic B H rate, and have therefore been neglected.

Since Λ is antisymmetric in p_+ and p_-, with a symmetric setup like that of this experiment, when integrating over the detector acceptance in order to get the mass distribution, the interference term (6) does not contribute. However, if each event is entered into a mass plot with the weight sign $(|\vec{p}_+|\theta_+ - |\vec{p}_-|\theta_-)$ (θ_+ being the projected angle on the horizontal plane of the positron with respect to the photon beam, and θ_- being that of the electron), only the interference effect contributes to the yield. When the Bethe-Heitler amplitude is found to be much larger than that of the

Compton process, as in this experiment, the interference plot is a much more sensitive way of looking for structures than the invariant mass plot.

2. - EXPERIMENTAL SET-UP AND DATA REDUCTION. -

The detail of the spectrometer[7] is shown in Fig. 1. The bremsstrahlung photon beam, produced by the 7.2 GeV DESY electron synchrotron and focussed to a spot size 10×35 mm^2, passes

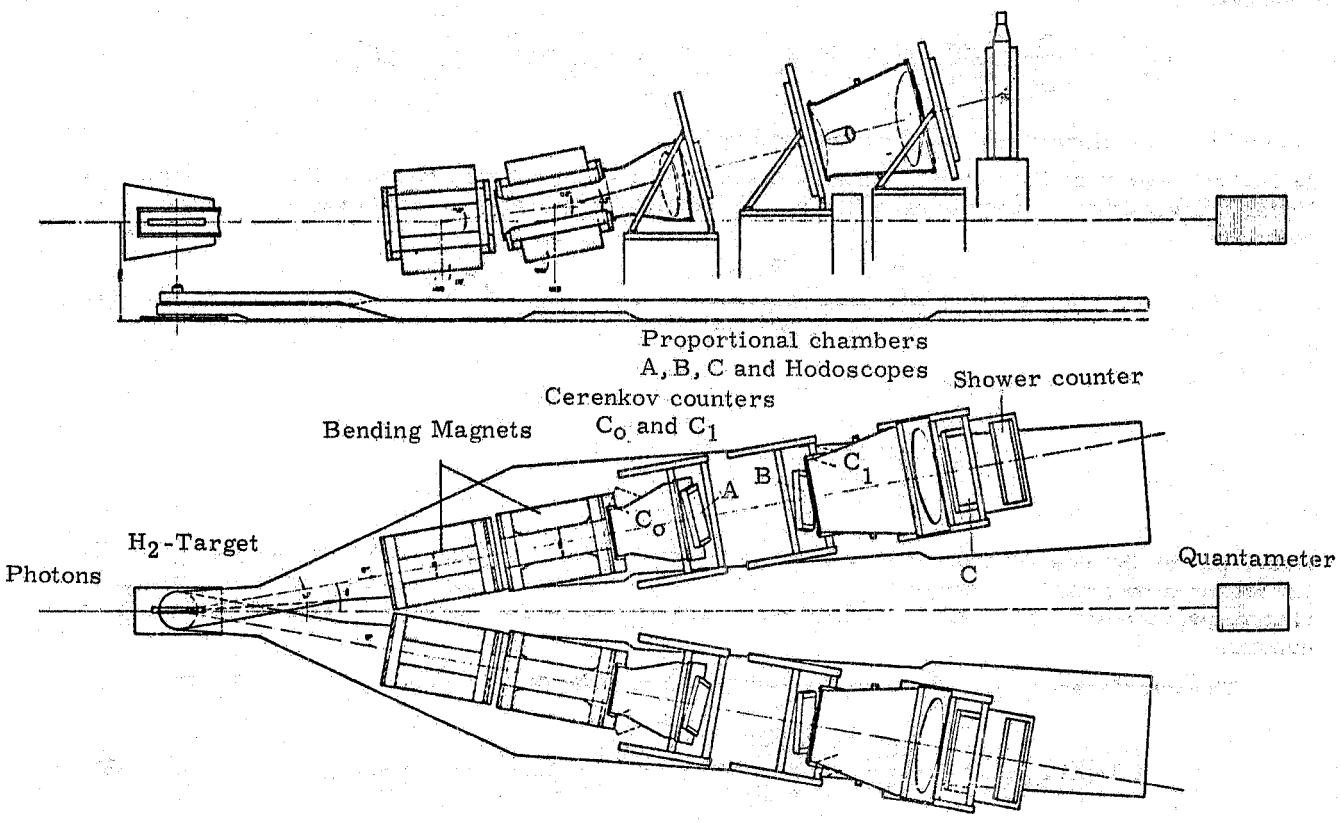

Fig. 1 - Side and plan views of the spectrometer.

through a liquid hydrogen target 100 cm long and 5 cm in diameter. Beam intensity is monitored by a Wilson-type quantameter whose calibration is known to $\pm$ 2%. Three telescopes, two looking at the H_2 target and one at a thin mylar window in the beam path, monitor the stability of the quantameter. The spectrometer is mounted on two platforms pivoting about the target in the horizontal plane from -10^o to a maximum of $+20^o$. The observed production angles of the produced pairs can thus be varied on either side of the incident photon beam. The central spectrometer momentum is chosen to be 2700 MeV. The bending plane is perpendicular to the production plane. This optimizes the mass resolution, since opening angle and momentum are measured independently of each other. The pair mass M is obtained from the positron and electron momenta p_+ and p_- and the opening angle θ_{12} of the pair by:

$$M^2 = 2(E_+E_- - p_+p_- \cos\theta_{12}) + 2\,m_e^2 \quad .$$

In each arm, two DESY MA magnets with the gap enlarged to 50 cm to increase the spectrometer acceptance, bend a 2700 MeV particle vertically by 13.8^o. Fig. 2 shows the p-φ acceptance of each arm. With the magnets positioned as in the spectrometer, the magnetic field has been mapped at 10^5 points with a three dimensional Hall probe to a relative accuracy of $\sim 10^{-4}$. During the experiment, the magnet current is held constant to approximately one part in 10^4.

Two threshold Cerenkov counters, C0 and C1, are used in each arm to identify electrons. To reduce the possibility of triggering on those pions which produce knock-on electrons in C0, this counter is located inside the second magnet. C0 is filled with 80% A + + 20% O_2 at atmospheric pressure. We have found[8] that this mixture scintillates very little, even less than H_2 or CO_2. The Cerenkov light is focused by a 3 mm thick precision spherical mirror, followed by a parabolic mirror, onto a XP2041 photomultiplier. An average of twelve photoelectrons are produced when an electron passes through the Cerenkov counter. The measured efficiency of C0 was better then 0.99 for all useful trajectories, as shown in Fig. 3. C1 is filled with CO_2 at atmospheric pressure. The efficiency of C1 has been measured in single arm runs to be better than 99.5%. The pulse height spectrum of C0 for reconstructed pairs is shown in Fig. 4, showing a very clean electron signal.

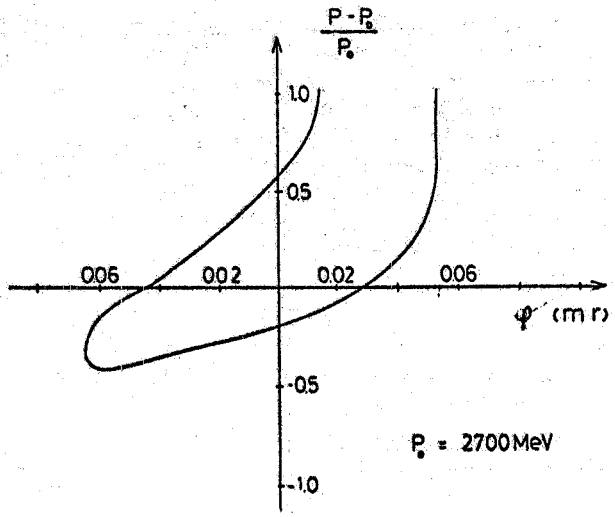

Fig. 2 - p - φ acceptance of one spectrometer (p_0 = central spectrometer momentum; φ = = vertical angle). The smearing effect of the extended target is included.

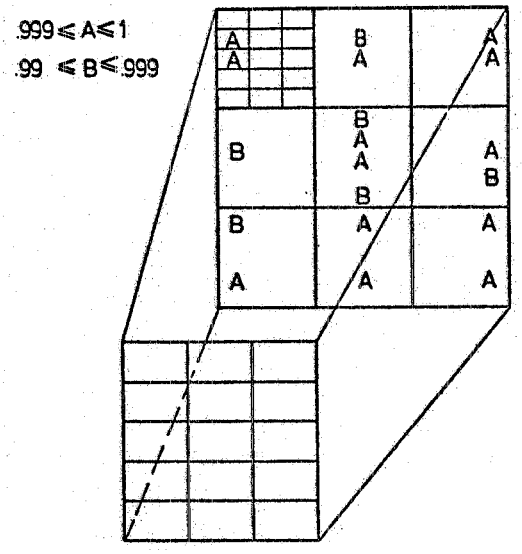

Fig. 3 - Efficiency map of a Cerenkov counter C0 over the useful phase space. Each of the fifteen sectors of the entrance face has been projected nine times over the corresponding section of the rear face. An efficiency larger than 0.99 was found in all cases (for simplicity, the efficiency is quoted only in a few areas in figure).

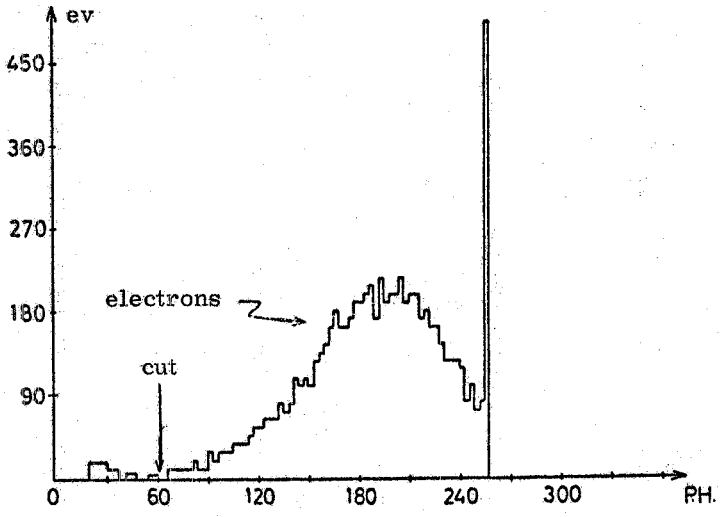

Fig. 4 - Experimental pulse height spectrum in a counter C0 for a sample of events (reconstructed left-right pairs). The cut used to define good electrons is also shown.

Shower counters are used at the end of each spectrometer arm to further discriminate against charged hadrons. Each shower hodoscope is split into seven elements. Each element is a lead-lucite sandwich of 12 radiation lengths.

Behind the magnets are three banks of hodoscope counters A, B, and C, and proportional wire chambers to measure the momentum p and the angles ϑ and φ of each particle. The space resolu-

tion is determined by the chambers. Each chamber has 2 orthogonal sense planes with a wire spacing of 2 mm. Each chamber is rotated by 10^{o} with respect to the preceding one to disentangle ambiguities in multitrack triggers. The time resolution is determined by the hodoscopes. Hodoscopes A and B comprise two 8-counter planes each. The scintillator strips are rotated by 45^{o} with respect to the chamber wires to further improve the resolution of ambiguities in the track reconstruction. These counters are 1.5 and 3 mm thick respectively, in order to reduce multiple scattering. The timing of the signal of each hodoscope counter relative to the main trigger is registered for each event. After correcting each hodoscope time-of-flight for the particle position in the counter, the rejection of accidental tracks in the chambers is improved by a factor of 20.

During the runs, the voltages of all counters are periodically monitored, and kept constant to within $\pm$ 1 V. The timing of all hodoscopes and the gain of the shower and the Cerenkov counters are checked by the computer with pulsed light diodes on each counter. The operation of each of the PWC amplifiers is also monitored by the computer with a set of pulsers capacitively coupled to the chamber sense wires.

The on-line signature of an electron pair is given by the coincidence (within $\pm$ 15 ns) of the four Cerenkov counters and the two shower hodoscopes. When a trigger occurs, the following information is recorded on tape: the pulse heights of the triggering counters, the TOF's of the triggering counters and of the hodoscope counters relative to the trigger signal, and the addresses of the fired PWC wires. The relative timing of the two C0 counters for electron pairs is shown in Fig. 5. The pulse height of the shower counters as a function of the electron momentum is shown in Fig. 6. The event distribution as a function of the shower pulse heights in the two arms is shown in a scatter diagram in Fig. 7.

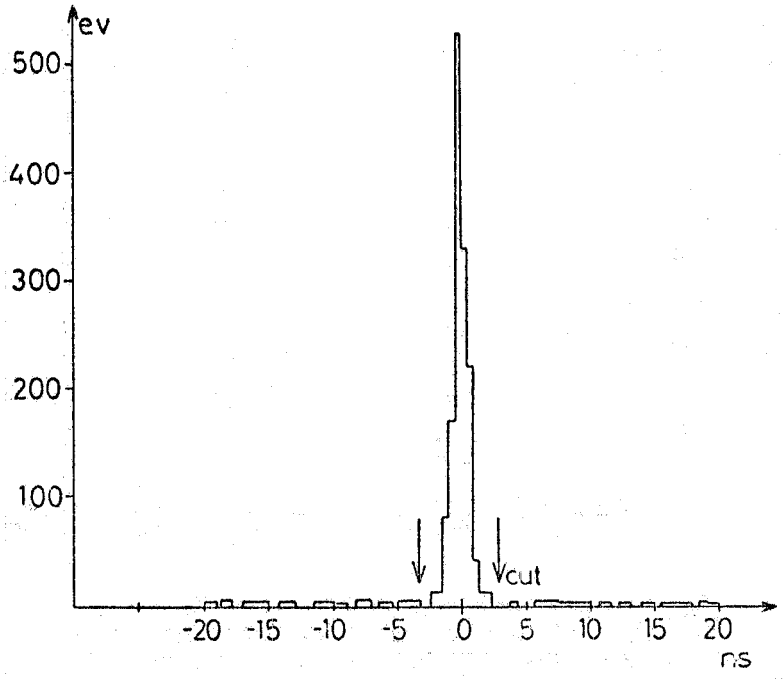

Fig. 5 - Time-of-flight spectrum between the two C0 Cerenkov counters for electron pairs. Cuts used to define a good pair are also shown.

Trajectories are reconstructed if at least four PWC planes in each arm are fired. Fig. 8 shows the χ^2 distribution of the reconstructed tracks. A cut is applied, and tracks with a χ^2 greater than 15 are rejected. In the reconstruction of the trajectories, the proper counters in the hodoscopes are checked against. If more than two counters fail to fire, or have bad timing, the track is rejected. Using this criterion, less than 1% of the good events is estimated to be lost. The track is then extended into the shower hodoscope, whose corresponding counter is required to have a signal.

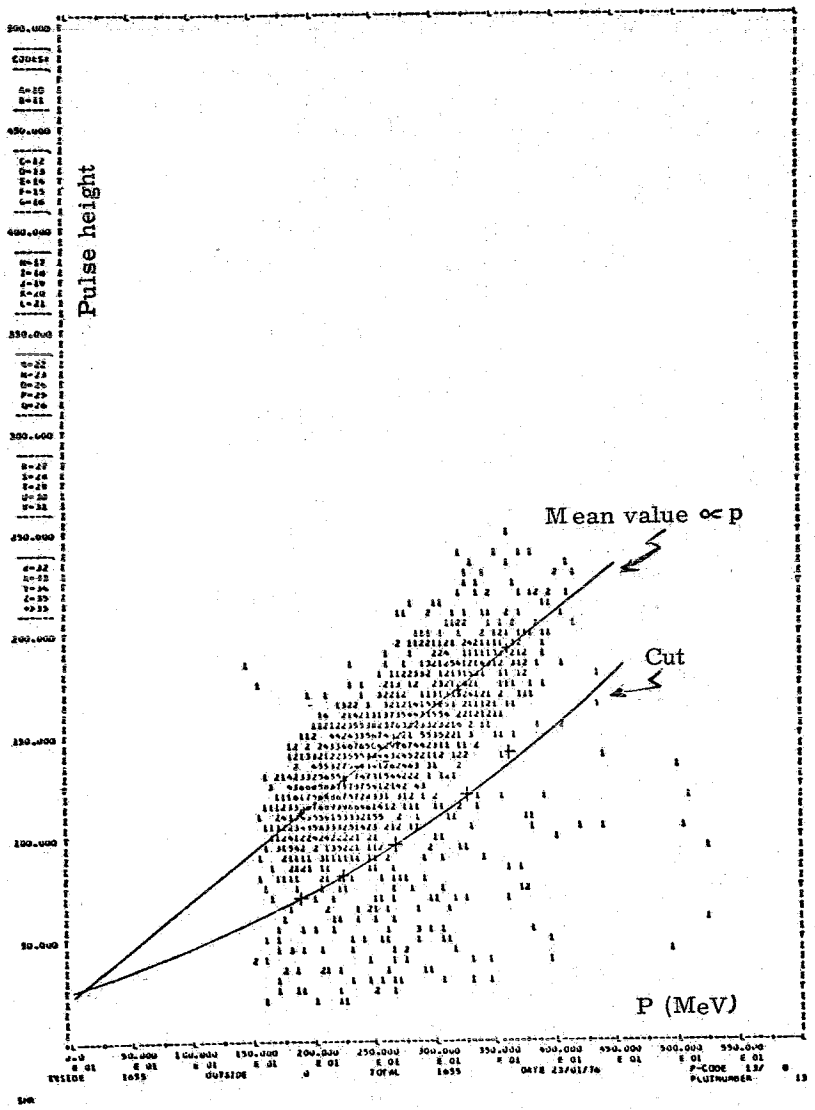

Fig. 6 - Pulse height spectrum versus momentum for a sample of detected pairs at $\theta = 16^{o}$ after correction for attenuation in the counter. The cut applied to define good electrons is shown. The relative resolution is measured to be $\pm 0.35/\sqrt{E}$ (FWHM) and the cut is applied two standard deviations below the mean value.

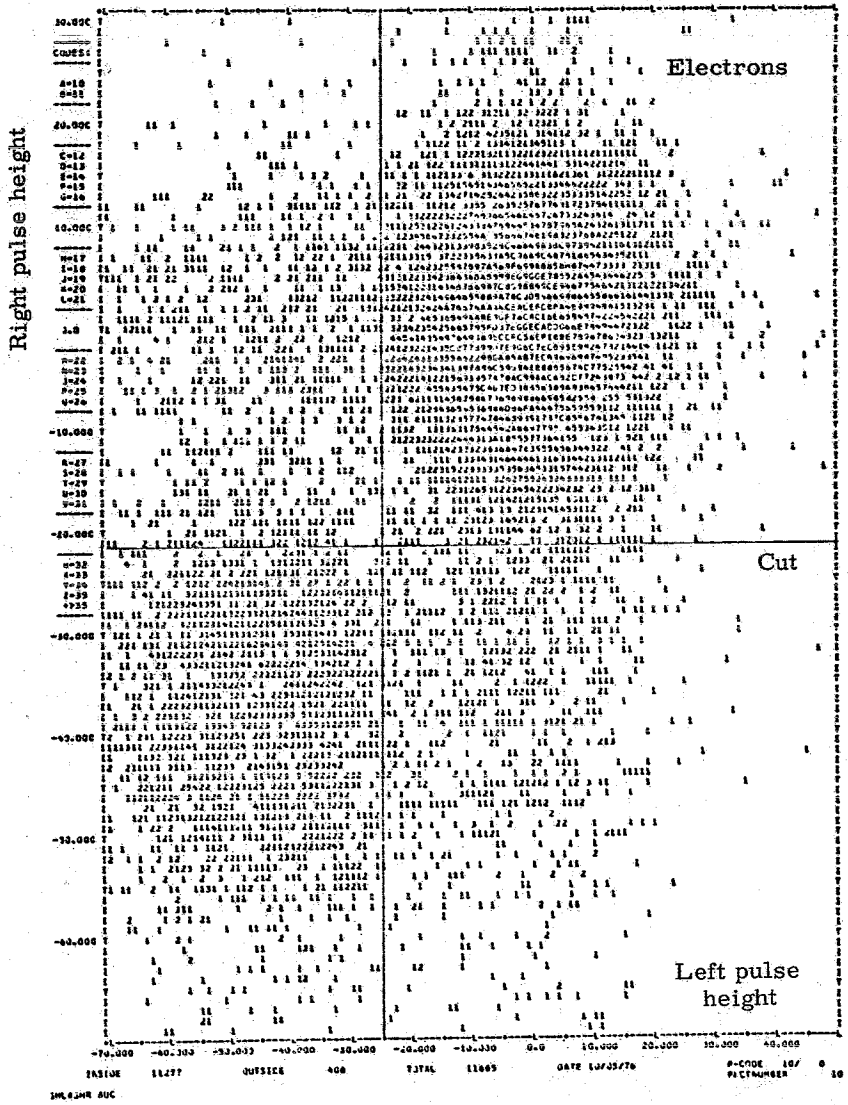

Fig. 7 - Event distribution versus the pulse-heights in the two shower counters. The cuts applied to define good electrons (larger pulse heights in both counters) are also shown. Pulse heights are normalized to the particle momentum and are expressed in units of one tenth of the FWHM expected resolution for that momentum.

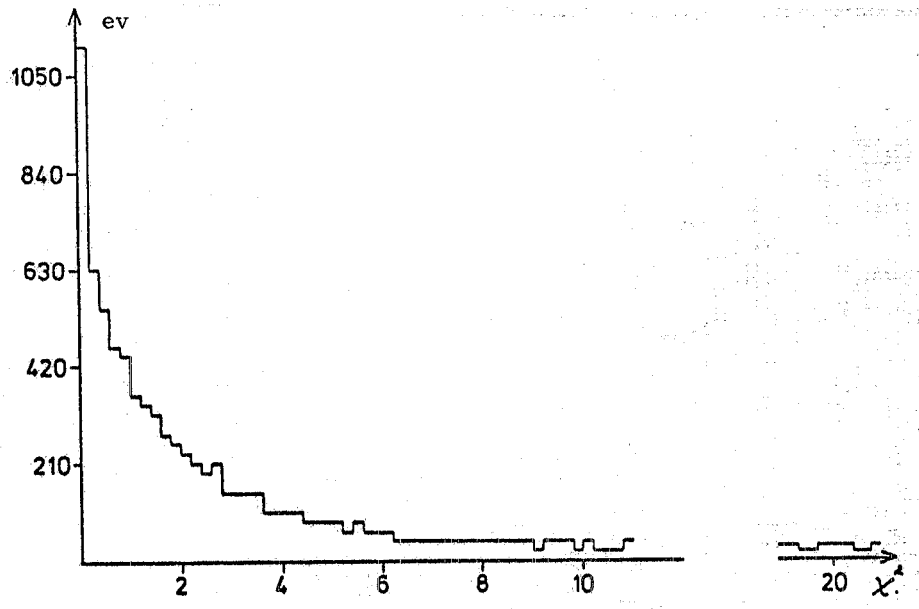

Fig. 8 - χ^2 distribution for reconstructed trajectories. Trajectories are rejected if $\chi^2 \geq 15$.

The momenta of the two tracks of an event are calculated by tracing the trajectories in the wire chambers back through the measured magnetic field, and by insisting that they meet on the horizontal plane containing the beam axis. The source distribution on this plane is shown in Fig. 9. Two independent programs for the event reconstruction from the PWC tracks have been used. The agreement is better than 1% in the reconstruction of events, and better than 0.1% in the e-pair mass.

The cuts applied in the off-line analysis to the left-right TOF, to the pulse-height in the shower counters and to the target dimensions are shown in Figs. 5, 6 and 9 respectively. With the adopted pulse height cuts, the hadron contamination is estimated to be less than 2%, and the electron-pair loss also less than 2%. Correction for accidentals is $\sim$ 0.5% after TOF and target cuts. The loss due to target cuts is $\sim$ 1%. The loss due to TOF cuts was found to be $\sim$ 8%. This is estimated by studying the TOF of the trigger counters one versus the other, and also independently by flashing the light diodes of all triggering counters during beam bursts. Empty target correction was found to be negligibly small.

To keep radiative corrections and bremsstrahlung losses constant, the central momentum of the spectrometer and the top energy of the beam were held fixed through the entire experiment. The full mass range to be covered in the experiment was spanned by varying the spectrometer angles.

Data have been taken at four angular settings with the two spectrometers positioned symmetrically at 13, 15, 16 and 19 degrees with respect to the beam. The mass acceptance for the spectrometer at these four settings is shown in Fig. 10. During the runs, the polarity of each arm was set alternatively for positrons and electrons. At each setting, the same amount of equivalent quanta was accumulated for each polarity in order to cancel out possible effects of minor asymmetries.

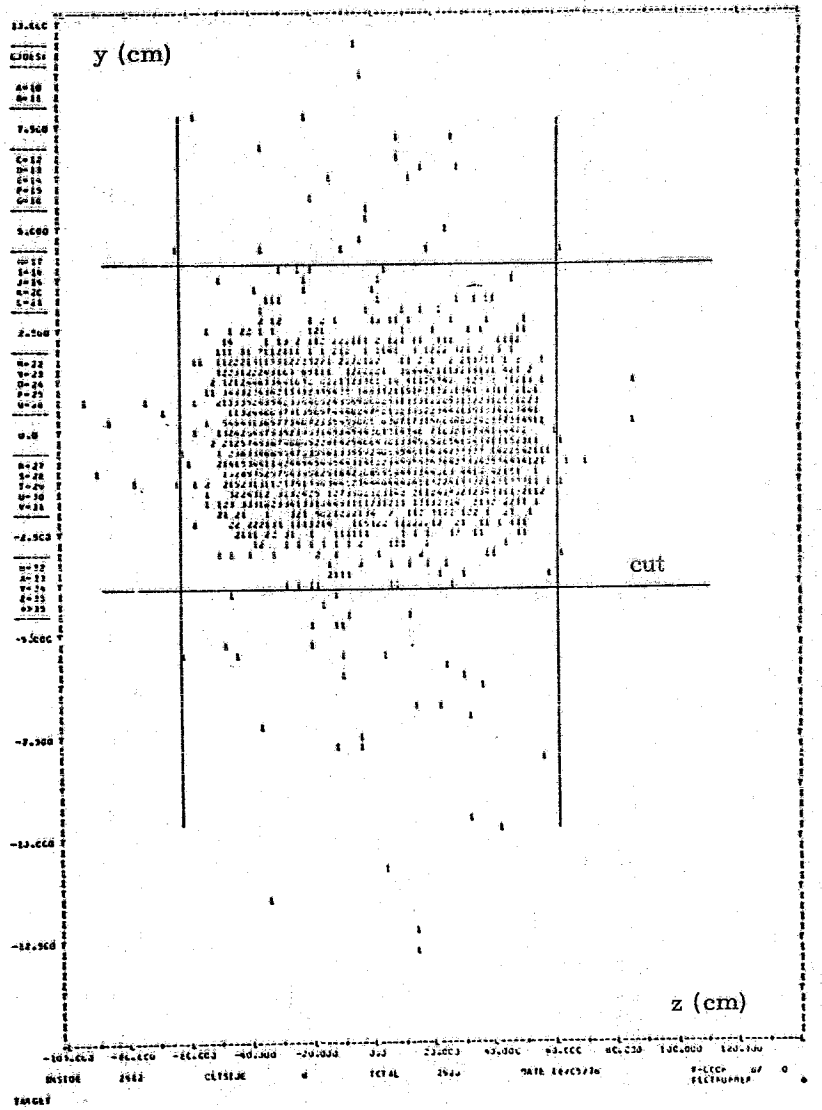

Fig. 9 - Plan view of the target as reconstructed by the horizontal projections of the trajectories of electron pairs. The y-z cuts applied in the analysis are indicated. According to Montecarlo calculations, 2/3 of the events outside the cuts (≃ 1.5% of the total sample) are due to failures of reconstruction programs, while according to TOF studies one concludes that the remaining 1/3 is due to accidental electron-positron coincidences.

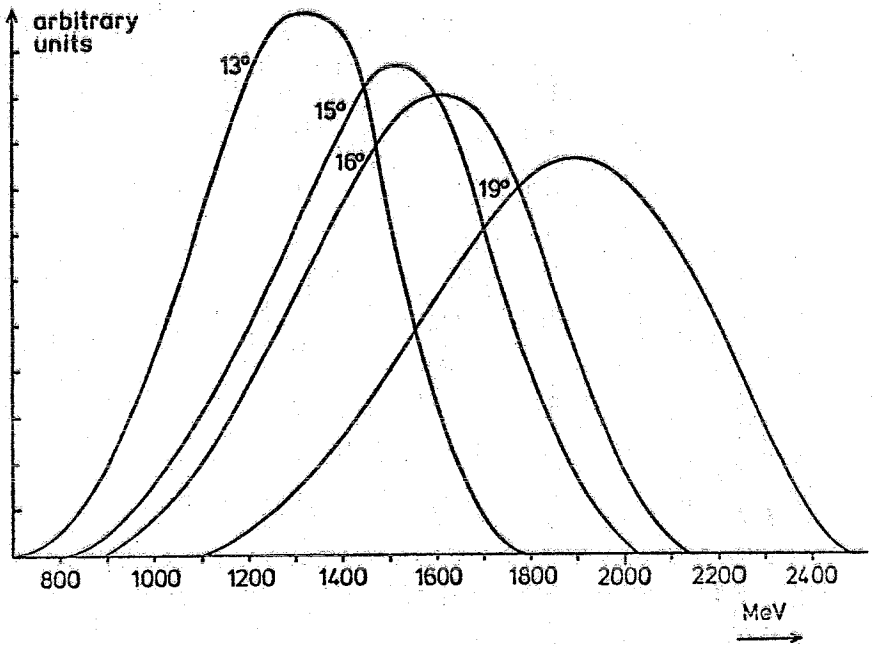

Fig. 10 - Acceptance in electron-pair mass for different angular settings of the spectrometers, integrated over the bremmstrahlung beam of 7.2 GeV top energy.

3. - EXPERIMENTAL RESULTS. -

Fig. 11 shows the measured e^+e^- mass distribution at the four angular settings. The parameters used in the Monte Carlo calculation to generate ϱ, ω, and Φ are listed in Table I. The expected Φ-meson rate has been calculated by taking radiative corrections ($\sim$ - 12%) into account, following ref. (9). The vector meson contribution in the accepted mass range is essentially due to the Φ production superimposed on the ϱ-tail. Table II summarizes the various contributions to the e^+e^- yield.

TABLE I - Parameters used in the various Monte Carlo calculations.

	M MeV	Γ MeV	$\left.\frac{d\sigma}{dt}\right\|_{t=0}(\gamma p \to Vp)$ $\mu b\ GeV^{-2}$ (asymptotic)	b (slope) GeV^{-2}	$BR \cdot \left.\frac{d\sigma}{dt}\right\|_{t=0}^{(x)}$ $\mu b\ GeV^{-2}$	φ degrees
ϱ	770	150	$120^{(11)}$	$7.8^{(11)}$	$4.27 \times 10^{-3(12)}$	$11.8^{o(13)}$
ω	783	10	$12.5^{(14)(+)}$	$7.2^{(14)}$	$0.904 \times 10^{-3(12)}$	$52.8^{o(15)}$
Φ	1020	4.2	$2.8^{(16)(o)}$	$5.5^{(16)}$	$1.07 \times 10^{-3(12)}$	$25^{o(17)}$
ϱ'	1550	300	$10^{(18)}$	$5.6^{(18)}$	$5.73 \times 10^{-5(19)}$	25^o

(x) $BR_{v \to e^+e^-} = \frac{\alpha^2}{12} \frac{4\pi}{\gamma_v^2} \frac{m_v}{\Gamma_v}$;

(+) We use an energy dependent fit to the data of Ref. (14) ;

(o) We use an energy dependent fit to the data of Ref. (20).

TABLE II - Computed and measured yields of e^+e^- pairs.

Source \ Spectrometer angle	13^o	15^o	16^o	19^o
QED elastic	9108 ± 128	5992 ± 82	2582 ± 35	242 ± 4
QED inelastic	646 ± 7	526 ± 6	237 ± 3	22 ± 0.3
QED radiative corrections	-683 ± 10	-460 ± 6	-202 ± 3	-20 ± 0.3
$\varrho + \omega + \Phi$ production	1192 ± 76	528 ± 46	169 ± 15	6 ± 0.2
Total expected yield	10263 ± 221	6586 ± 140	2786 ± 56	250 ± 4.8
Total measured yield	10302 ± 101	6739 ± 82	3027 ± 55	307 ± 18 (*)
Number of eq. quanta collected	3.07×10^{16}	5.64×10^{16}	4.1×10^{16}	2.0×10^{16}

(*) A systematic error of $\pm 5\%$ must be added to the errors quoted in this row due to uncertainties in proton electric and magnetic form factors, quantameter calibration, event losses, accidentals, etc.

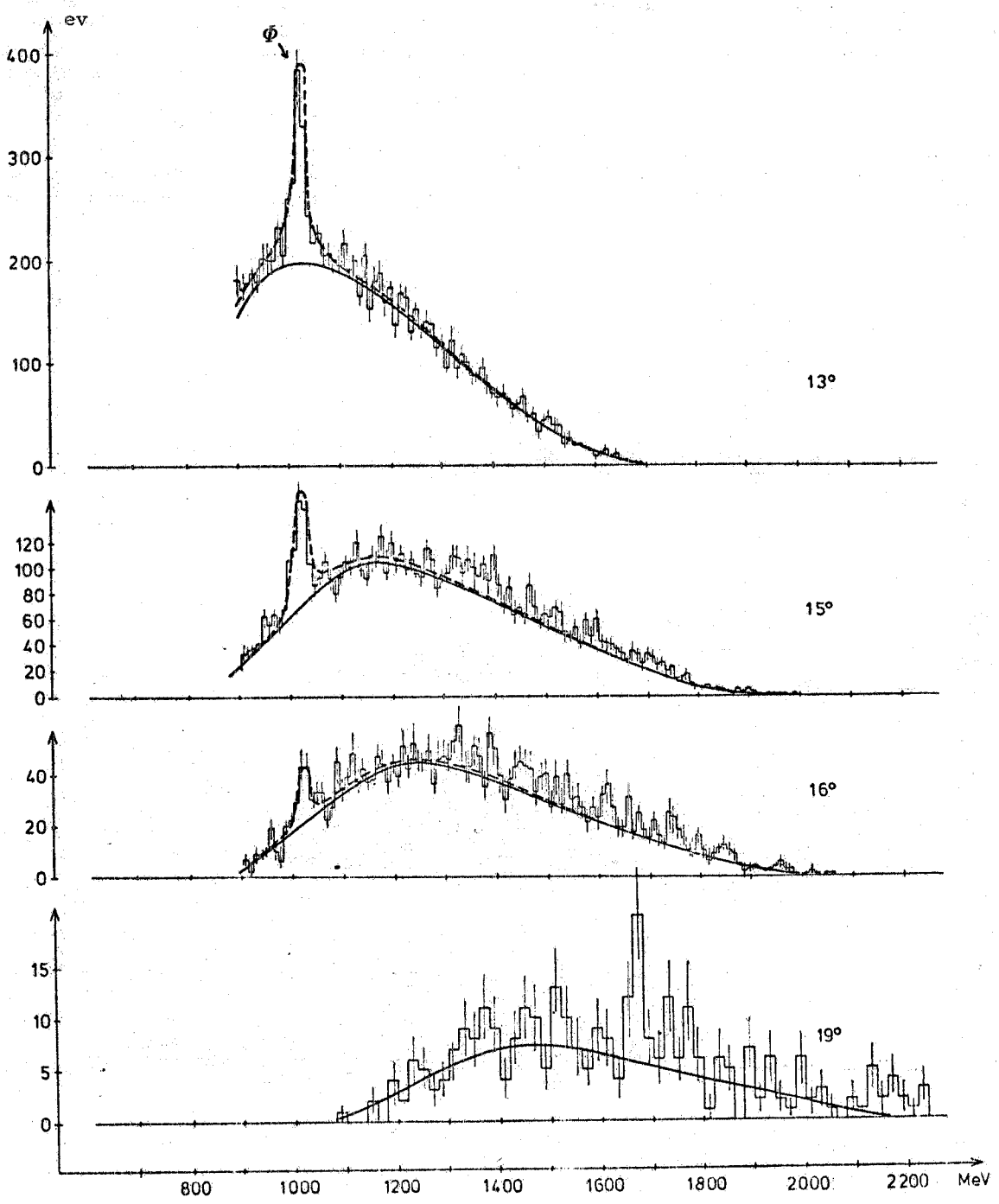

Fig. 11 - Mass spectrum of e^+e^- pairs at the different angular settings. The solid line represents the QED yield. The dashed line indicates the ϱ, ω and Φ contribution. Computed yields are normalized to the same number of equivalent quanta.

Fig. 12 shows the invariant mass distribution, after removing QED contributions. The good agreement between expectation and experiment over the full mass range at 13° indicates that all systematic incertitudes have been understood and taken into account satisfactorily. However, data taken at larger angles (viz. with acceptance centered at larger mass values) show deviations from the expected yield at masses larger than the Φ mass, which increase with increasing opening angle. At the Φ mass, however, one always gets the same sort of agreement as at $\theta = 13^{o}$. We observe that the Compton production of vector mesons behaves as $N_C \approx p^2 e^{bt}$, where $p^2 = (p_+ + p_-)^2$, and therefore does not strongly depend on the opening angle θ of the e^+e^- pair, whereas the B H contribution is $N_{BH} \approx p^{-2}\theta^{-7}$ and decreases very fast with increasing θ. Therefore this anomaly is suggestive of Compton production of vector mesons with mass larger than the Φ mass. For

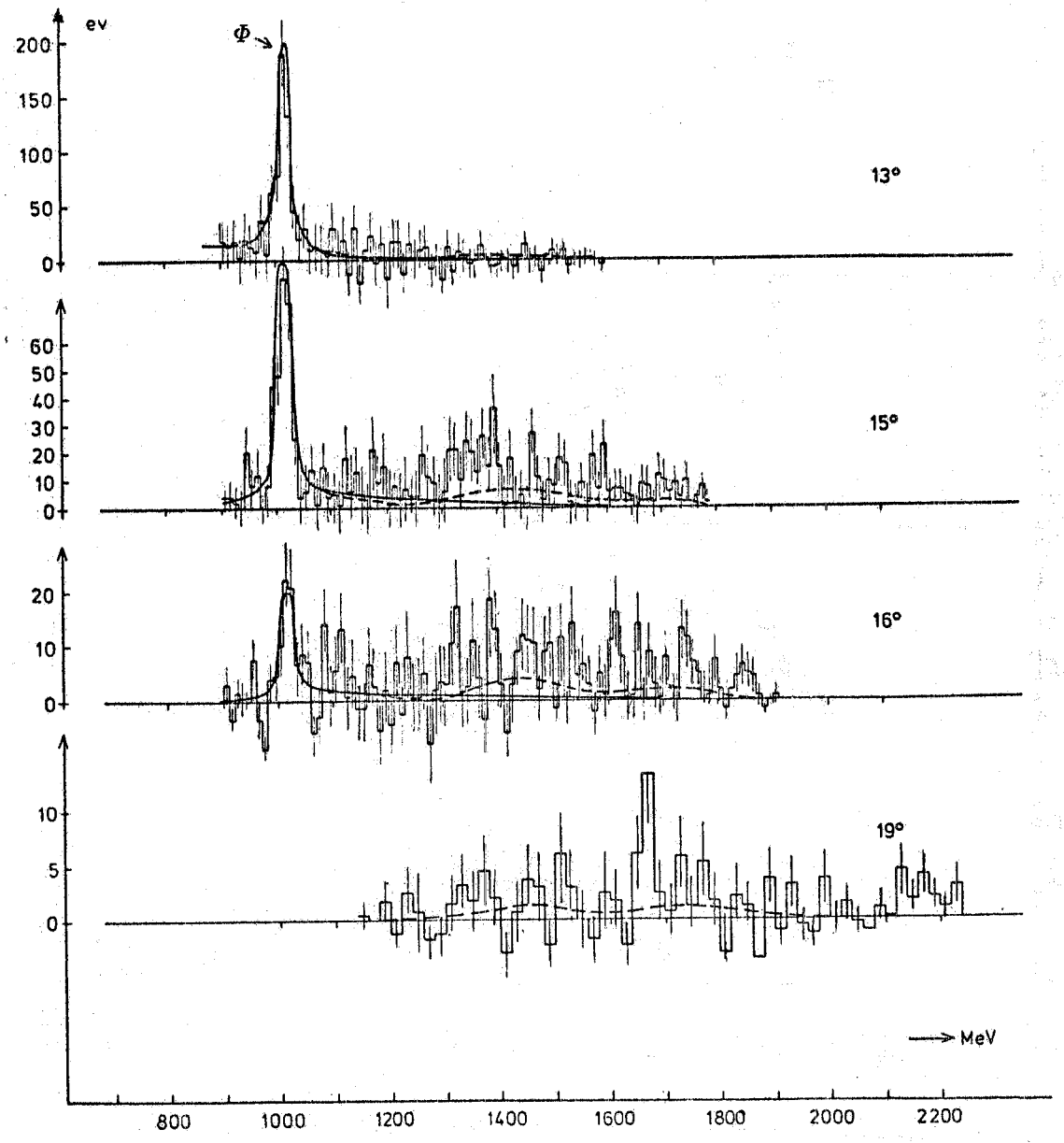

Fig. 12 - Yield of e^+e^- pairs with QED contributions removed. The solid line indicates the contribution from ϱ, ω, and Φ. The dashed line indicates what would be contributed by two resonances at 1400 MeV and 1700 MeV generated according to the parameters of Table III.

instance the data at the 19° setting for masses $\approx$ 2150 MeV is very different from expectation. For 2100 $\leq$ M $\leq$ 2240 MeV, 1.8 ± 1.4 events are expected and 18 events are found.

Fig. 13 shows the interference pattern at the four angular settings. The dashed curve shows the expected distributions for ϱ, ω, and Φ interference using the parameters of Table I.

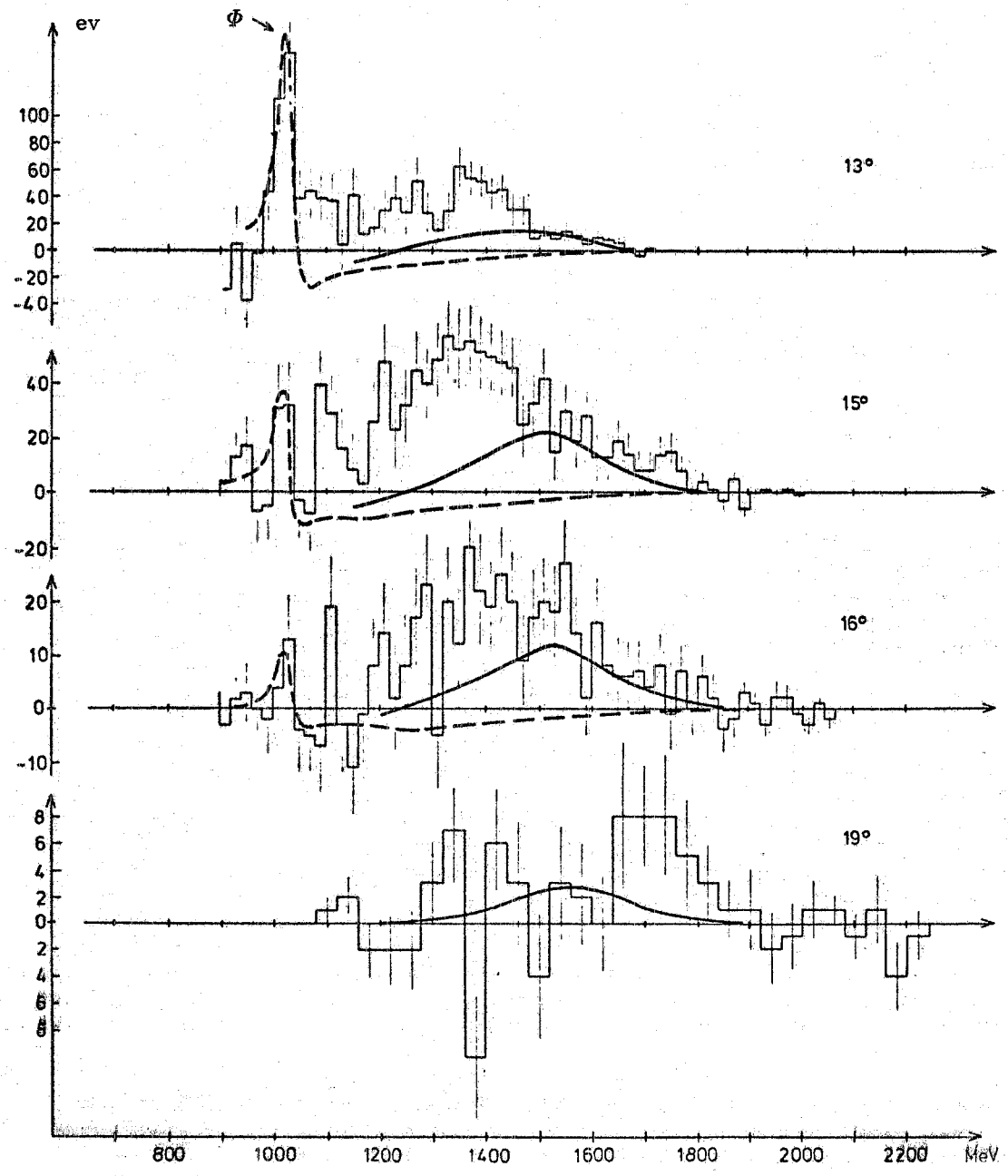

Fig. 13 - Interference spectra for the same events displayed in Fig. 12. The dashed line represents the ϱ, ω, and Φ interference pattern, predicted by Monte Carlo calculation with the parameters of Table I. The solid line is the ϱ"(1600) contribution as expected from the measured[18, 19, 21, 22, 23, 24] parameters (also listed in Table I). Predicted and observed yields are normalized to the same number of equivalent quanta.

Fig. 14 illustrates how in a given mass bin ($1000 \leq M \leq 1040$ MeV) the interference signal is obtained. To check that the observed asymmetry is a real effect, we have analyzed the approximatively 3000 events at $\theta = 13^{o}$ and 15^{o}, which fullfill all requirements for a good pair except that

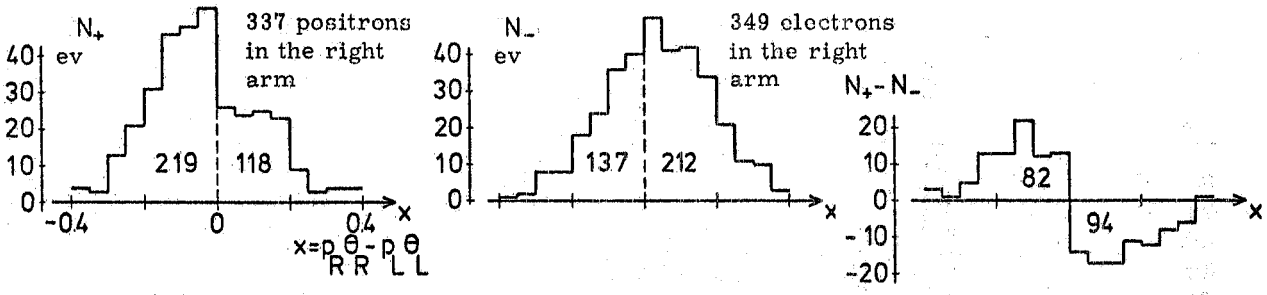

Fig. 14 - This figure illustrates in detail how the interference signal is obtained, for the particular case $1.0 \leq M \leq 1.04$ GeV and $\theta = 13^{o}$. At $x < 0$, the positrons dominate over the electrons by 219 - 137 = 82, and viceversa at $x > 0$ (212 - 118 = 94 electrons more then positrons). The total interference is 82 + 94 = 176 events. $P_{R(L)}$ and $\theta_{R(L)}$ are the lepton momentum and angle respectively, in the right (left) spectrometer. $\theta_{L(R)}$ is the projected production angle on the horizontal plane.

their pulse height in the shower counters is smaller than the cut applied to define good electrons. As seen in Fig. 15, the result is consistent with no asymmetry at any mass value.

In the $\theta = 15^{o}$ and 16^{o} interference plots of Fig. 13 one observes a narrow structure at 1.1 GeV. On the other hand, because of the mass resolution of ~ 20 MeV FWHM, the strong Φ signal in the 13^{o} data makes the separation of the signal at 1.1 GeV not as distinct. It however still shows up as a shoulder for $M > M_{\Phi}$. Summing up from 1080 MeV to 1120 MeV, the deviation from the expected distribution due to ϱ, ω, and Φ around 1.1 GeV is 128 ± 27 events in the 13^{o} data, 93 ± 19 in the 15^{o} data, and 19 ± 10 in the 16^{o} data. This corresponds to a total of seven standard deviations. Assuming a mass of 1100 MeV, a width of 20 MeV, and a slope of 6 GeV^{-2}, which is consistent with the data, it is found that a value of $BR \cdot (d\sigma/dt)\ (\gamma p \rightarrow Vp) = 3.7 \times 10^{-5}\ \mu b\ GeV^{-2}$ can account for the signal in all three angular settings, as shown in Fig. 16. Fig. 16 also allows to set a lower limit to the width of the 1100 structure. Indeed, for a given interference signal, the peak production rate in the invariant mass distribution is almost inversely proportional to the width of the structure, as long as the width is smaller than the adopted mass bin. From the signals in the mass plot which are expected for widths of the 1100 structure of 1, 5 and 20 MeV, as shown in Fig. 16, we estimate that the width is between 5 and 30 MeV. It has to be pointed out that the statistical significance of the 1100 signal is related to the adopted ϱ-tail parametrization and Φ-photoproduction phase. Fig. 17 shows the predicted interference patterns at $\theta = 15^{o}$ when the ϱ-tail is described by the Jackson relativistic formula[10], and the Φ-production phase is assumed to be zero. We find that within this model the evidence for the new 1100 structure is put into question more than in any assumption that we have been able to think of. On the other hand, this model is unable to predict correctly the interference pattern around the Φ-mass.

In all plots of Fig. 13, there is a large excess of events in the mass region from 1200 to 1800 MeV. Although this data cannot lead to a unique interpretation, we have searched for possible underlying physical processes by fitting the experimental interference distributions with one, two, three and four resonances, with unknown mass, width, production cross-section and phase in the mass range between 1200 and 1800 MeV.

The fitted resonance parameters are given in Table III and the fitted curves are shown in Figs. 18 and 19. The overall agreement of each fit with the data is quite good. We consider that this is an important internal consistency check of the data taken at different angular settings.

Although no fit can be preferred on a purely statistical base, we would like to point out a

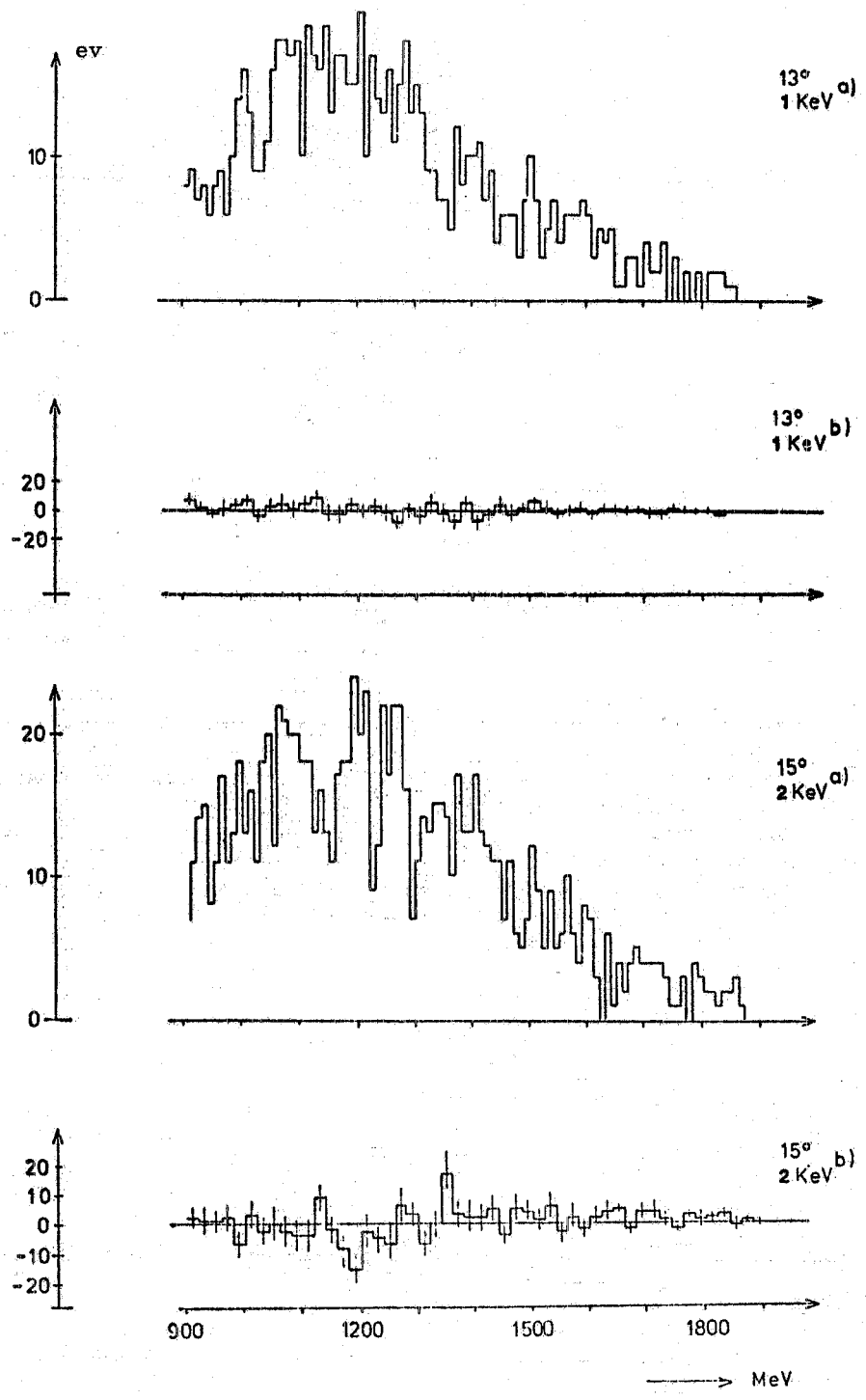

Fig. 15 - Mass and interference spectra for hadron pairs. A hadron pair is defined as a pair generated within the fiducial cuts defining the target and having the proper time of flight, but with pulse height in both arms lower than the cuts used to define electrons (see Fig. 7). Not only the Φ-signal has disappeared but also the data are consistent with no interference signal at any mass-value.

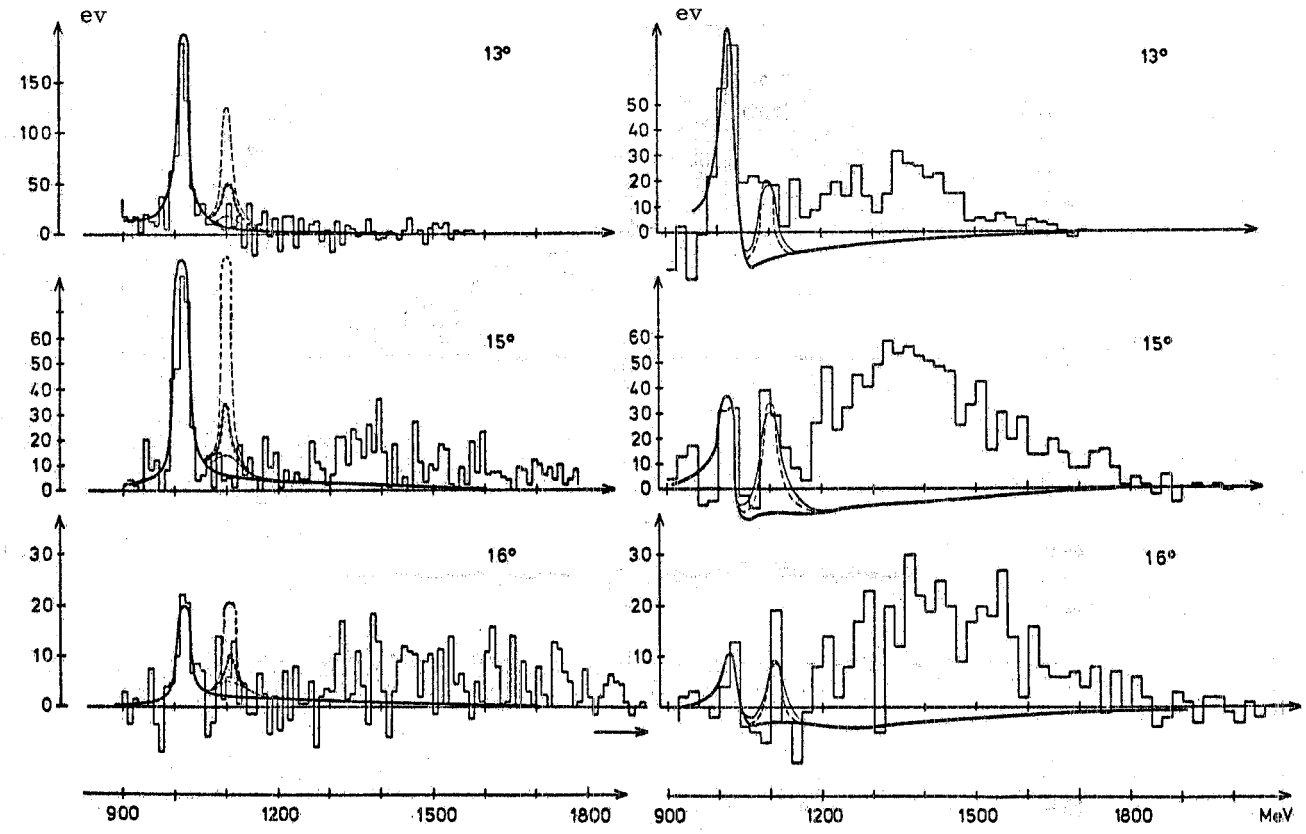

Fig. 16 - Mass spectrum with QED removed (left side) and interference pattern (right side) at 13°, 15° and 16°. The solid line is the ϱ, ω, and Φ contribution. The thin solid line, the crossed-dash line and the dashed line represent the contribution of the 1100 MeV state where the width is assumed to be 20, 5 and 1 MeV respectively. $BR \cdot (d\sigma/dt)(\gamma p \rightarrow Vp)$ is scaled down almost inversely proportional to the width in order to keep essentially constant the interference contribution predicted by the Monte Carlo calculation.

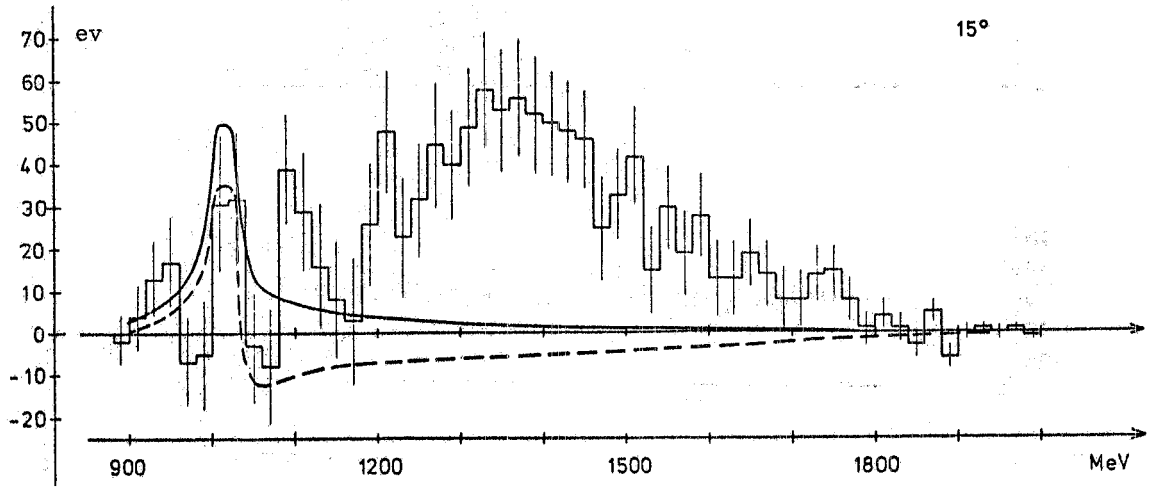

Fig. 17 - Measured interference pattern at 15°. The dashed line represents the ϱ and Φ contribution, as calculated according to the parameters of Table I. The ϱ-tail is described, as explained in Section 1, by the resonance formula with a constant width Γ_o. The solid lines is the ϱ and Φ contribution, assuming the Φ phase equal to zero and describing the ϱ production term by the resonance formula with a mass dependent width:

$$\Gamma_\varrho = \frac{m_\varrho}{m} \left(\frac{m^2 - 4m_\pi^2}{m_\varrho^2 - 4m_\pi^2} \right)^{3/2} \Gamma_o \quad (10).$$

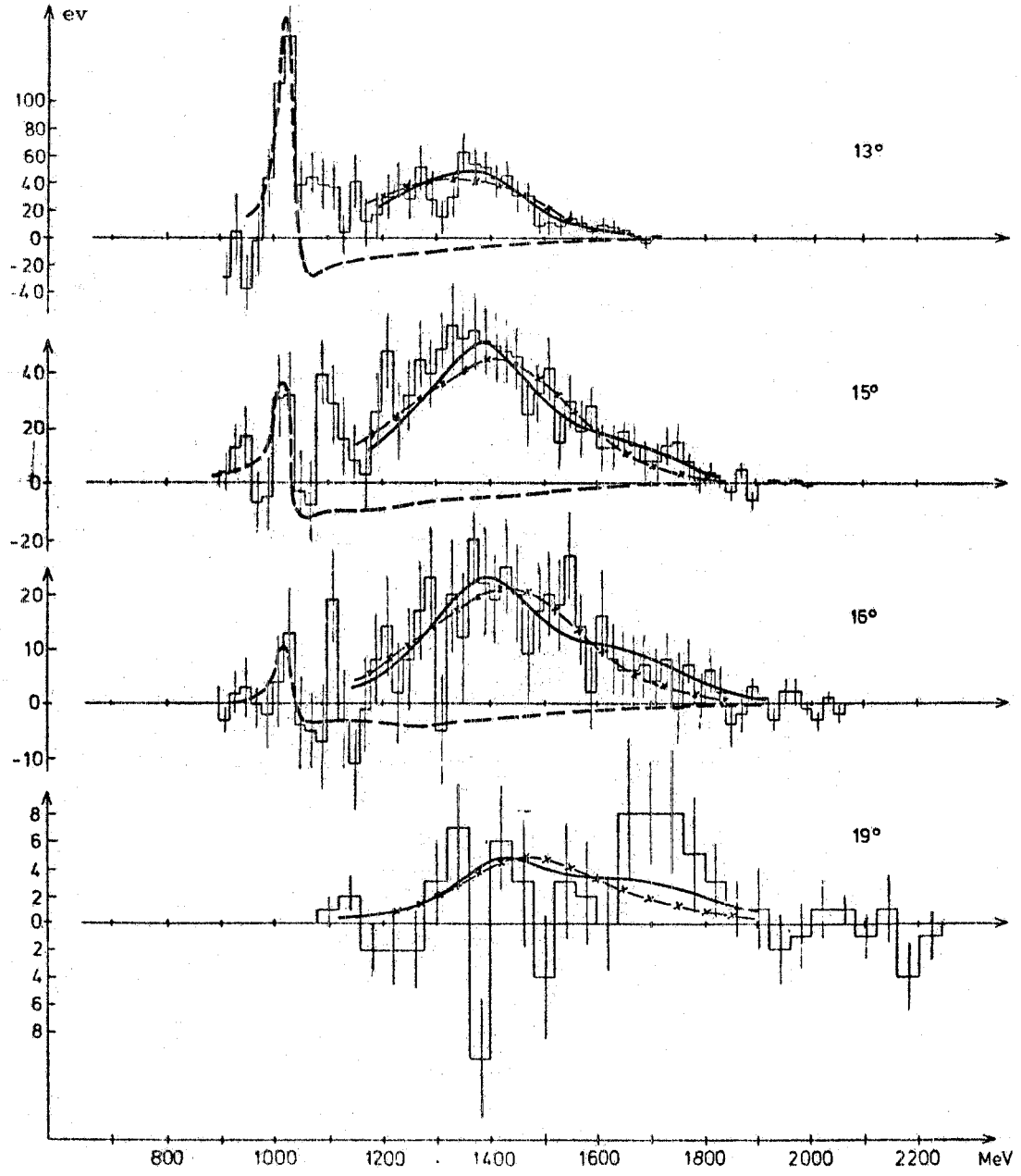

Fig. 18 - One resonance (crossed-dash line) and two resonance (solid line) fits to the interference data at M > 1200 MeV. The fitted parameters are given in Table III. The dashed line represents the ϱ, ω and Φ contribution.

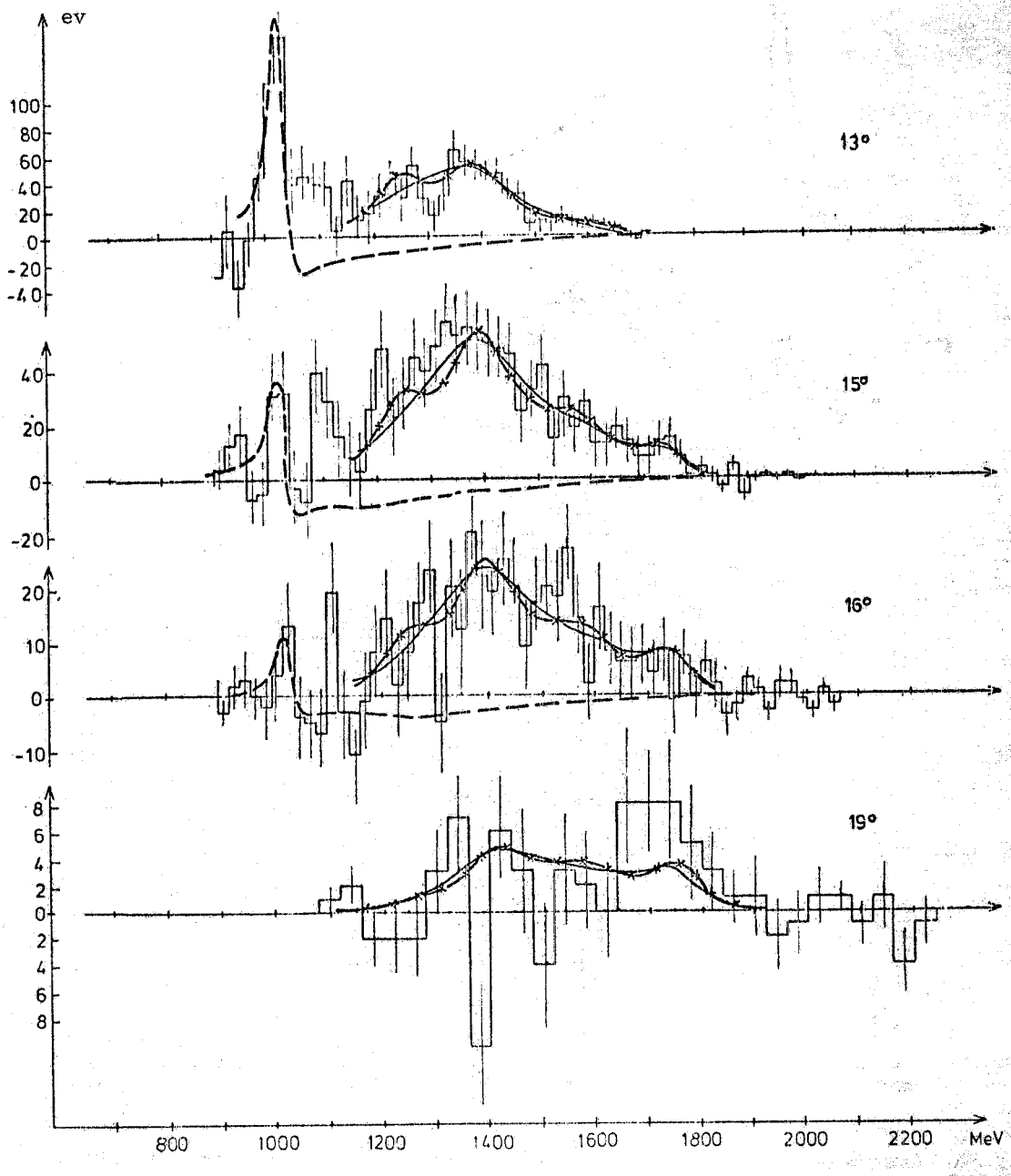

Fig. 19 - Three resonance (solid line) and four resonance (crossed-dash line) fits to the interference yield at M > 1200 MeV. The fitted parameters are given in Table III. The dashed line represents ϱ, ω and Φ contribution.

TABLE III - Parameters of the resonance fits to the interference signal in the mass range $1200 \leq M \leq 1800$ MeV(o).

	M_V (MeV)	Γ_V (MeV)	$\frac{1}{\gamma_V^2/4\pi}\frac{d\sigma}{dt}\Big\|_{t=0(\gamma p \to Vp)}$ μb GeV^{-2}	φ_V (degrees)	χ^2/degrees of freedom
1 res. fit	1443 ± 41	469 ± 82	16.6 ± 4.0	0.(+)	114/131
2 res. fit	1394 ± 11 1710 ± 24	245 ± 45 393 ± 105	3.5 ± 0.7 3.5 ± 0.3	6.2 ± 2.5 7.1 ± 8.0	99/126
3 res. fit	1381 ± 5 1600 ± 30 1760 ± 32	245 ± 15 430 ± 121 91 ± 89	3.2 ± 0.5 1.8 ± 0.7 0.15 ± 0.16	0 ± 1.5 7.0 ± 13.0 23.0 ± 23.0	98/122
4 res. fit	1253 ± 16 1401 ± 9 1549 ± 26 1766 ± 8	120 ± 38 134 ± 18 230 ± 21 139 ± 30	0.16 ± 0.1 1.0 ± 0.2 0.87 ± 0.25 0.6 ± 0.15	6.8(x) 11.0 ± 9.0 1.2 ± 6.0 29.0 ± 5.0	93/119

(o) The slope value b_V is assumed to be 6 GeV^{-2} for all resonances. This value is found to be well consistent with the data at all masses.
(+) In this particular fit the phase was kept fixed to zero, since otherwise an unphysical negative phase was found by the fit.
(x) Kept fixed in the fit.

number of features which are of interest. In the one resonance fit, one observes an excess of events at $M > 1640$ MeV. Adding up data at all angles, the excess for $1640 < M < 1840$ MeV is a 4.5 s.d. effect. In addition, the fitted values $M = 1443 \pm 41$ MeV and, more important, $\frac{1}{\gamma_V^2/4\pi}\frac{d\sigma}{dt}\Big|_{t=0}(\gamma p \to Vp) = 16.6 \pm 4.0$ b GeV^{-2}, are quite far from the previously measured values of the only vector meson which is so far well established[18,19,21,22,23,24], the ϱ"(1600), the mass of which is between 1550 and 1600 MeV and $\frac{1}{\gamma_V^2/4\pi}\frac{d\sigma}{dt}\Big|_{t=0} = 2.5$ b GeV^{-2}. An unsucessfull attempt to account for our data with a ϱ"(1600) with these parameters (see in Table I) was shown in Fig. 13. We have found in particular that, for any value of $\varphi_{\varrho"}$, the integrated area below the solid line does not vary by more than 20%. We conclude that no single resonance like structure, as the ϱ"(1600), can properly account for our data.

In the two resonance fit the agreement between predicted and experimental yields is appreciably improved, and one cannot find any local systematic disagreement as the one discussed above. These facts favour the existence of two vector mesons, with masses ~ 1400 and ~ 1700 MeV (see Table III).

Only the three resonance fit is able to indicate a resonance at $M \sim 1600$ MeV, which could be identified as the ϱ". The quality of the fit, however, is in no respect improved over that of the two resonance fit. The fit therefore would deserve consideration only if one takes the attitude that the ϱ"(1600) is so well established, that it must be included in the fit. The parameters of the ϱ" and of the two additional resonances, which would be indicated in this case, are listed in Table III.

In the four resonance fit, an additional resonance is indicated at $M \sim 1250$ MeV, again with negligible statistical evidence. Similar to what was observed above, this fit can be of interest only if one believes that in addition to the ρ"(1600), also the ϱ'(1250) is well established by other expe-

riments[25-33], such that it must be included in the fit. The parameters of the ϱ', ϱ'' and of the two new resonances which would be indicated in this case are listed in Table III.

4. - CONCLUSIONS. -

We quote in summary the results of our search for photoproduced vector mesons decaying into e^+e^- in the mass region $0.9 \leq M \leq 2.2$ GeV as follows. A new structure of mass ~ 1100 MeV and width $5 \leq \Gamma \leq 30$ MeV is strongly indicated by the data. Within the only model which can reproduce the interference pattern in the Φ-region, the 1100 MeV signal has a statistical significance of 7 s.d. Between 1200 and 1800 MeV, although one cannot reach any firm conclusion, the rather complex interference pattern is indicative of more than one underlying resonances. The most economical interpretation suggests two new broad structures at 1400 and 1700 MeV, while no compelling evidence for either the $\varrho''(1600)$ or the $\varrho'(1250)$ is contained in the data. If one assumes that the $\varrho''(1600)$, or both the $\varrho''(1600)$ and the $\varrho'(1250)$, have been established by other experiments, such that they should be included in the fits, the data would still indicate the existence of two new structures at about 1400 and 1700 MeV.

We are grateful to Profs. H. Schopper, G. Weber and G. Bellettini who made this collaboration possible. The DESY Direktorium is also thanked for the continuous support extended to this experiment. We are also indebted to Prof. S. Ting and his MIT-DESY Group, who exploited for many years at DESY the experimental approach that we continue with this experiment.

We acknowledge a number of interesting discussions that we had with Profs. H. Joos, M. Krammer, P. Söding, G. Bellettini and M. Greco, and P. Berger, H. Lenzen, K. Löffler and U. Rehder for skillful technical assistance. Drs. S. Mancuso, P. Shah, S. Vaccaro are thanked for the help given at the beginning of the data taking.

The warm cooperation of the Accelerator Group, of the Technical Support Groups and of the Computer Center of DESY has been essential for the success of this experiment.

REFERENCES. -

(1) - S. D. Drell and J. D. Walecka, Ann. Phys. 28, 18 (1964).
(2) - M. L. Perl, T. Braunstein, J. Cox, F. Martin, W. T. Toner, B. D. Dieterle, T. F. Zipf, W. L. Lakin and H. C. Bryant, Phys. Rev. Letters 23, 1191 (1969).
(3) - S. Mehrotra and M. Roos, Helsinky Univ. Report ISBN 951-45-0635-9 (1975).
(4) - M. Damashek and F. Gilman, Phys. Rev. D1, 1319 (1970).
(5) - B. Huld, Phys. Rev. 168, 1782 (1968).
(6) - J. Brodsky and J. G. Gillespie, Phys. Rev. 173, 1011 (1968).
(7) - S. Bartalucci, S. Bertolucci, C. Bradaschia, M. Fiori, D. Fong, P. Giromini, S. Guiducci, T. Mc Corriston, C. Rippich, M. Rohde, A. Sermoneta and L. Trasatti, DESY Report 76/43 (1976).
(8) - S. Bertolucci, C. Bradaschia, T. Mc Corriston, P. Giromini, C. Rippich, M. Rohde and S. Vaccaro, DESY Report 75/16 (1975).
(9) - F. Ehlotzky and N. Ritter, Nuovo Cimento 55A, 181 (1968).
(10) - J. D. Jackson, Nuovo Cimento 34, 1644 (1964).
(11) - G. Wolf, Cornell Conference Proceedings (1971), pag. 205.
(12) - J. Lefrancois, Cornell Conference Proceedings (1971), pag. 52.
(13) - H. Alvensleben, U. Becker, M. Chen, K. J. Cohen, R. T. Edwards, T. M. Knasel, R. Marshall, D. J. Quinn, M. Rohde, G. H. Sanders, H. Schubel and C. C. Ting, Nuclear Phys. 25B, 342 (1971).

(14) - J. Ballam, G. B. Chadwick, R. Gearhart, Z. G. T. Guiragossian, M. Menke, J. J. Murray, P. Seyboth, A. Shapira, C. K. Sinclair, I. O. Sillikorn, G. Wolf, R. H. Milburn, H.H. Bingham, W. B. Fretter, K. C. Moffeit, W. J. Podolsky, M. S. Rabin, A. H. Rosenfeld and R. Windmolders, Phys. Rev. Letters 24, 1364 (1970).

(15) - H. Alvensleben, U. Becker, W. K. Bertram, M. Chen, K. J. Cohen, R. T. Edwards, T. M. Knasel, R. Marshall, D. J. Quinn, M. Rohde, G. H. Sanders, H. Schubel and S. C. C. Ting, Nuclear Phys. 25B, 333 (1971).

(16) - H. J. Behrend, J. Bodekamp, W. P. Hesse, D. C. Fries, P. Heine, H. Hirschmann, W. A. Mc Neely, A. Markou and E. Seitz, Phys. Letters 56B, 403 (1975).

(17) - H. Alvensleben, U. Becker, W. Busza, M. Chen, K. J. Cohen, R. T. Edwards, P. M. Mantsch, R. Marshall, T. Nash, M. Rohde, H. F. W. Sadrozinsky, G. H. Sanders, H. Schubel, S. C. C. Ting and Sau-Lan Wu, Phys. Rev. Letters 27, 444 (1971).

(18) - H. H. Bingham, W. B. Fretter, W. J. Podolsky, M. S. Rabin, A. H. Rosenfeld, G. Smadja, G. Y. Post, J. Ballam, G. B. Chadwick, Y. Eisenberg, E. Kogan, K. C. Moffeit, P. Seyboth, I. O. Sillikorn, H. Spitzer and G. Wolf, Phys. Letters 41B, 635 (1972).

(19) - G. Barbarino, M. Grilli, E. Iarocci, P. Spillantini, V. Valente, R. Visentin, F. Ceradini, M. Conversi, L. Paoluzi, R. Santonico, M. Nigro, L. Trasatti and G. T. Zorn, Lett. Nuovo Cimento, 3, 689 (1972).

(20) - H. J. Behrend, J. Bodekamp, W. P. Hesse, D. C. Fries, P. Heine, H. Hirschmann, W. A. Mc Neely, A. Markou, and E. Seitz, Tbilisi Conference Proceedings (1976).

(21) - M. Davier, I. Derado, D. E. C. Fries, F. F. Lin, R. F. Mozley, A. Odian, J. Park, W. P. Swanson, F. Villa and D. Yount, Nuclear Phys. 58B, 31 (1973).

(22) - G. Alexander, O. Benary, J. Gandsman, D. Lissauer, A. Levy, Y. Oren and L. M. Rosenstein, Phys. Letters 57B, 487 (1975).

(23) - W. Y. Lee, Slac Conference Proceedings (1975).

(24) - B. Hyams, C. Jones, P. Weilhammer, W. Blum, H. Dietl, G. Grayer, W. Koch, E. Lorenz, G. Lütjens, W. Männer, J. Meissburger, W. Ochs, U. Stierling and F. Wagner, Nuclear Phys. 64B, 134 (1973).

(25) - R. Anderson, O. Gustavson, J. Johnson, D. Ritson, B.H. Wiik, W. G. Jones, D. Kreinick, F. Murphy, and R. Weinstein, Phys. Rev. D1, 27 (1970).

(26) - E. Rabe, DESY Report 71/2 (1971).

(27) - J. Ballam, G. B. Chadwick, V. Eisenberg, E. Kogan, K. C. Moffeit, I. O. Skillicorn, H. Spitzer, G. Wolf, H. H. Bingham, W. B. Fretter, W. J. Podolsky, M. S. Rabin, A. H. Rosenfeld, G. Smadja and P. Seyboth, Nuclear Phys. B76, 375 (1974).

(28) - V. Alles Borelli, M. Bernardini, D. Bollini, P. L. Brunini, E. Fiorentino, T. Massam, L. Monari, F. Palmonari, F. Rimondi, G. Valenti and A. Zichichi, Nuovo Cimento 30A, 136 (1975); Phys. Letters 46B, 261 (1973).

(29) - M. Conversi, L. Paoluzi, F. Ceradini, S. D'Angelo, M. L. Ferrer, R. Santonico, M. Grilli, P. Spillantini and V. Valente, Phys. Letters 52B, 493 (1974).

(30) - G. Cosme, A. Coureau, B. Dudelzac, B. Greland, B. Jean-Marie, S. Jullian, D. Lalanne, F. Laplanche, G. Parrour, R. Riscalla, P. H. Roy and G. Szklarz, Orsay-LAL Report 1287 (1976).

(31) - V. M. Aulchenko, G. I. Budker, I. V. Vassermann, I. A. Koop, L. M. Kuradze, V. P. Kutovoy, A. P. Lisenko, S. I. Mishnev, E. V. Pakhtuseva, S. I. Sidorov, A. N. Skrinsky, G. M. Tumaikin, A. G. Khabakhpashev, A. G. Chilingarov, Y. M. Shatunov, B. A. Shwartz and S. I. Eidelman, Tbilisi Conference Proceedings (1976).

(32) - G. Bassompierre, G. Binder, P. Dalpiaz, P. F. Dalpiaz, G. Gissinger, S. Jacquey, C. Peroni, A. Ruzza, M. A. Scheegans and L. Tecchio, Phys. Letters 65B, 397 (1976).

(33) - F. Frenkiel, C. Ghesquiere, E. Lillest, S. V. Ching, J. Diaz, A. Ferrando and L. Montanet, Nuclear Phys. 47B, 61 (1972).